Project No. 09-842

SiC Schottky Diode Detectors for Measurement of Actinide Concentrations from Alpha Activities in Molten Salt Electrolyte

Fuel Cycle R&D

Dr. Wolfgang Windl
The Ohio State University

Dan Vega, Federal POC
Michael Miller, Technical POC

NEUP Nuclear Energy University Programs
U.S. Department of Energy

Project Title: SiC Schottky Diode Detectors for Measurement of Actinide Concentrations from Alpha Activities in Molten Salt Electrolyte

Project Number: NEUP 09-842

Project Period: October 1, 2009 through October 31, 2012

Principal Investigators:

Dr. Wolfgang Windl
Professor, Department of Materials Science and Engineering
The Ohio State University
2041 College Road
Columbus, OH 43210
windl.1@osu.edu

Dr. Thomas E. Blue
Professor, Nuclear Engineering Program and Director, OSU Research Reactor Lab
The Ohio State University
201 West 19th Avenue
Columbus, OH 43210
blue.1@osu.edu

Organization: The Ohio State University, Columbus, Ohio.

Abstract:
In this project, we have designed a 4H-SiC Schottky diode detector device in order to monitor actinide concentrations in extreme environments, such as present in pyroprocessing of spent fuel. For the first time, we have demonstrated high temperature operation of such a device up to 500 ^{o}C, in successfully detecting alpha particles. We have used AM-241 as an alpha source for our laboratory experiments. Along with the experiments, we have developed a multi scale model to study the phenomena controlling the device behavior and to be able to predict the device performance. Our multi scale model consists of ab initio modeling to understand defect energetics and their effect on electronic structure and carrier mobility in the material. Further, we have developed the basis for a damage evolution model incorporating the outputs from ab initio model in order to predict respective defect concentrations in the device material. Finally, a fully equipped TCAD-based device model has been developed to study the phenomena controlling the device behavior. Using this model, we have proven our concept that the detector is capable of performing alpha detection in a salt bath with the mixtures of actinides present in a pyroprocessing environment.

Project Objective: This project was a collaborative effort between researchers from Materials Science and Engineering and Nuclear Engineering at The Ohio State University to investigate the use of SiC Schottky diode detectors for measuring the concentrations of actinides in the process stream for pyrochemical processing of spent nuclear reactor fuel, including device fabrication, testing, and a modeling-assisted study to unambiguously link damage to detector performance and model reliability and lifetime, which included an experimental and computational study of post-irradiation microstructural evolution as well as ab-initio based modeling of the detailed dependence of the electrical properties and detector signal on the damage.

Organization of the report: We begin with describing milestones proposed in the project and the respective achievements, followed by detail description of the work involved and by a list of resulting publications and presentations. Softcopies of papers, presentations etc. have been provided in the quarterly reports during the project period.

Milestones:

- Design of Schottky Diode Detector: We have successfully designed a 4H-SiC based Schottky diode detector by processing commercially available n-type SiC wafers from Cree Inc. The wafers had a background doping density of 10^{18} cm^{-3} and a low doped epitaxial region. Schottky contacts were deposited on the epilayer while the Ohmic contacts were deposited on the back side of the wafer. Ni-metal has been employed as base metal to develop the Schottky and Ohmic contacts. A series of experiments were performed to make the electrical connections to the detector such as with high temperature nickel paste, mechanical contacts etc. We established that among the examined methods, mechanical contacts were the most stable at high temperatures.
- High Temperature Detector Experiments: We have successfully demonstrated the successful operation of these SiC Schottky diode detectors for alpha particle detection from an Am-241 alpha source in our laboratory at high temperatures. This is the first ever report of alpha particle detection at temperatures as high as 500 ^{o}C. We have observed the peak positions to shift to higher channel numbers with increasing temperature, which we believe is due to reduction in the band gap of SiC with increasing temperature. The detector is ready to be tested inside the reactor lab.
- Characterization Experiments: We have characterized our detector using IV and CV measurements. Further we also performed EDS on some of the detectors to estimate the composition of the contact after metallization. An EELS study of a detector, pre- and post-irradiation detector still remains to be successfully completed.
- Damage Evolution Model: In collaboration with Dr. Pichler from the Fraunhofer Institute for Integrated Systems and Device Technology (IISB), Erlangen, Germany, we developed a continuum model within the PROMIS platform to apply to the SiC system. The Sentaurus Process Monte Carlo program has been applied to create the damage in the detector material, while the further damage evolution has been simulated with PROMIS.
- Ab-initio modeling: Using first principles modeling based on Density Functional Theory, we studied defect energetics, which are a necessary input for damage evolution modeling. We also simulated the electron loss near edge structures of the SiC material with various defects which on comparison with experimental EELS can give an identification of the types of defects present in the system, pre and post irradiation. Furthermore, we developed a self-consistent mobility calculation model to study the effect of the various defects on the electronic mobility in the material. This serves as an input for device modeling to understand and predict the device behavior with damage developed in the material during extended operation.

- Device modeling: A device model has been developed which is utilized to understand the key phenomena controlling the device output in order to predict the device behavior under irradiation in the pyroprocessing environment. Our device model proves the concept that by comparing the experimental results with the output of the device model, we can identify mixtures of actinides present in the environment. The modeling also showed clearly the resolution limits that the detectors have for cases where characteristic alpha-energies are too similar.

Detailed Description of the Tasks:

Detector Design:

A 4H-SiC based Schottky diode type of detector was fabricated using clean room processing. Two wafers were bought from Cree, Inc. Both were fabricated with a top epilayer grown thick enough to ensure that the active volume would be thicker than the range of Am-241 decay alpha particles when properly reverse-biased. Our clean room processing involved RCA wafer cleaning to remove any oxide layer present on the wafers as they were shipped. This was followed by deposition of metal contacts using thermal evaporation and subsequent annealing. We used Ni as the base metal for both Schottky and Ohmic contacts. Ni is known to form various silicides depending upon annealing conditions. These

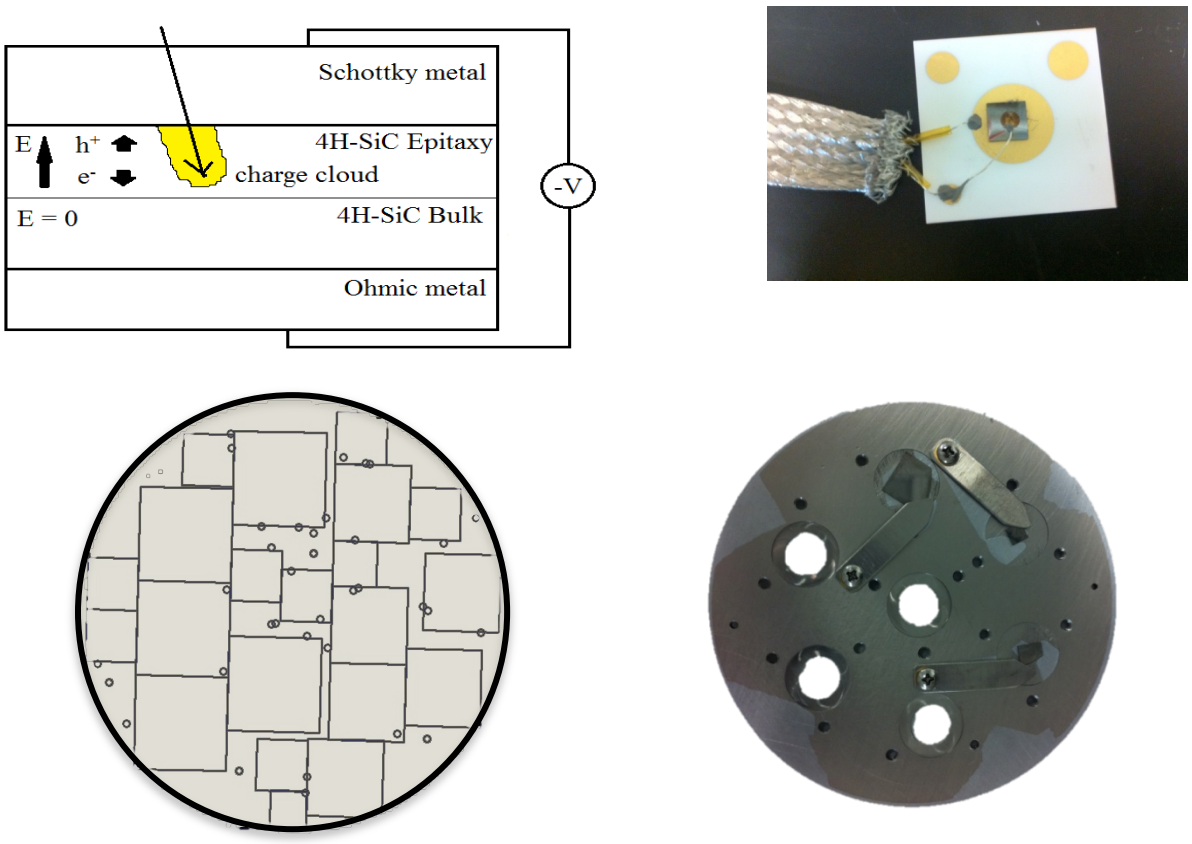

Figure 1: a) Schematic operation of a Schottky diode detector, (b) 4H-SiC based Schottky diode developed in our lab on an insulating alumina pad, with electrical connections made using nickel paste, (c) wafer dicing plan to ensure exclusion of micropipes from the active region of the diode, and (d) fabricated mask holder, showing 4 open metallization ports and 3 ports occupied by 4H-SiC samples.

silicides offer different work functions, so by proper design of the annealing process, the Schottky and Ohmic contacts can be developed. The procedure followed was first depositing Ni metal and annealing at 950 ^{o}C, flipping the sample over, placing a circular shadow mask in front of the sample, and then depositing Ni metal and annealing at 650 ^{o}C. The primary silicide phase which forms the Ohmic contact is Ni_2Si, while the primary silicide phase which forms the Schottky contact is $Ni_{31}Si_{12}$. Ni readily oxidizes at high temperature, so to protect the exposed metal during the high temperature tests, we deposited a thin layer of Ti for adhesion, followed by an oxidation-resistant thin layer of Au. Figure 1 (a) and (b) shows the schematic of the Schottky diode detector operation and a Schottky diode detector with Ni-paste connected wiring developed in our lab.

When shipping the wafer, Cree includes in the shipment a scan of material defects called micropipes. Micropipes affect the device performance adversely by causing breakdown at a lower voltage than the theoretical breakdown voltage. The wafer-dicing plan (Fig. 1(c)) was designed in order to ensure that micropipes were excluded from the active region of the detectors. Further, a mask (Fig. 1(d)) was designed to perform metallization on multiple wafer pieces with varying sizes of active region of the detector.

High Temperature Detection Experiments:

A bell jar high temperature spectroscopy setup was fabricated to perform alpha spectra and I-V measurements under vacuum, while allowing the detectors to be at a controlled temperature between room temperature and 800 $^{\circ}$C. The maximum temperature of the heater that was used sets the upper limit for temperature. This semiconductor heater was purchased from Blue Wave Semiconductor and installed on a stand in the bell jar. This was done to thermally isolate the heater from the bell jar structure, so that the low-temperature vacuum equipment would not be heated above its operational temperature.

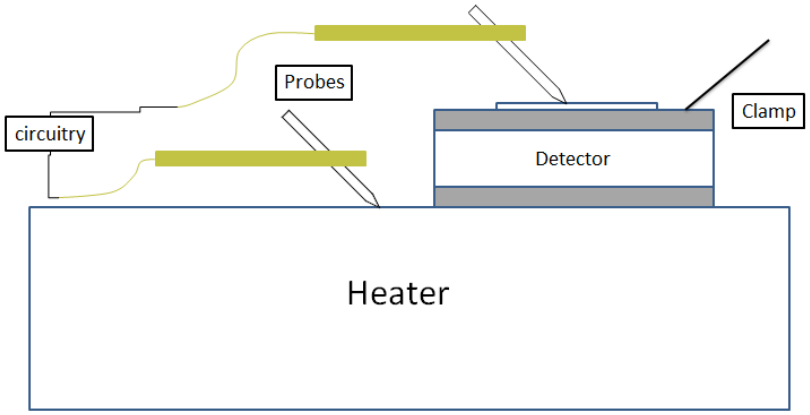

Figure 2: Illustration of a detector clamped onto the heater, and probe system allowing for repeatable electrical contact.

Control electronics were installed to turn off the counting system while the heater was energized, and turn it on when the heater was de-energized to minimize electrical interference. In order to resolve the technical issues, which became apparent during early testing, a mechanical clamp was used to press the detector directly onto the heater surface. An illustration of the final version of the electrical contacts, which are mechanical, is show in Figure 2.

A shutter was installed so that the alpha particles could be shielded from the detector, and an Ortec pulser could be used to characterize the electrical noise in the system. Two micropositioners were

purchased from Signatone, that allow for making electrical contact using purely mechanical force with Tungsten-based probes. The bell jar with outer shield removed is shown in Figure 3. A closeup of the detector placed in the testing location is shown in Figure 4.

Outside of the bell jar were two different sets of experimental equipment; one to take I-V measurements, and one to take alpha spectra measurements. The I-V measurement equipment consisted of a Keithley 2410 sourcemeter unit, and a Dell laptop for control and data acquisition. The alpha spectra measurement equipment consisted of an Ortec 142B charge-sensitive preamplifier, a Canberra DSA 2000, and the same Dell laptop for control and data acquisition. The Canberra DSA 2000 was controlled via a USB-based U3 Labjack data acquisition device, whose input was routed through the laptop. An illustration of the important features of the control, electrical heating, shielding, and alpha signal can be seen in Figure 5.

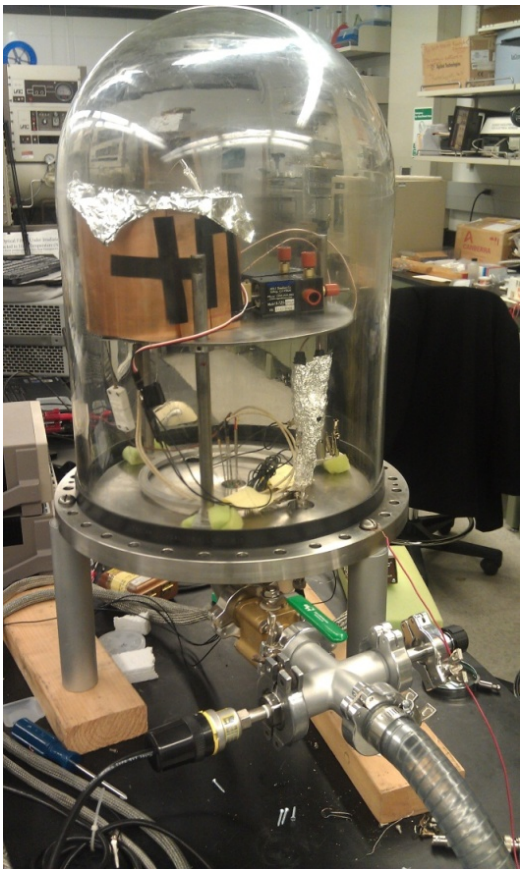

Figure 3: Picture of bell jar without the outer shield. The vacuum inlet is seen in the lower right hand corner, with thermocouple pressure sensor, air vent, and hand-actuated ball valve. The copper shield with aluminum top seen on the stand in the bell jar acts as a guard surface.

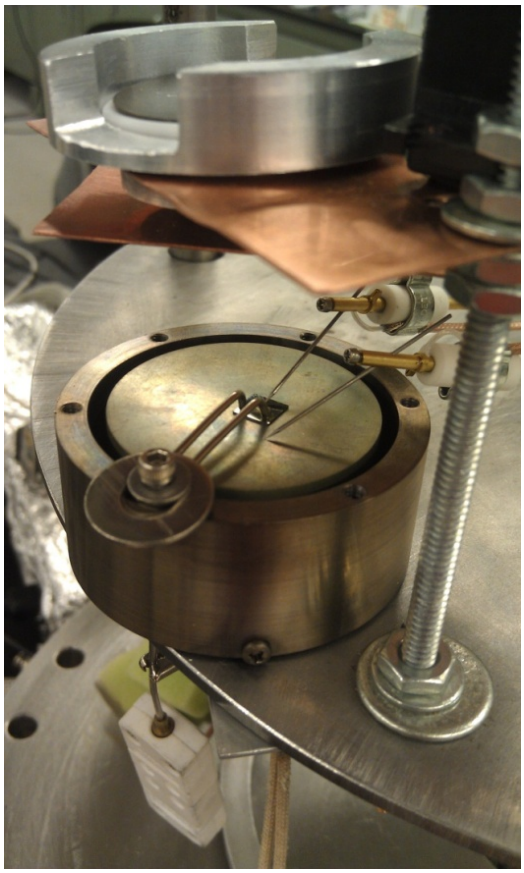

Figure 4: Close-up picture of a 4H-SiC detector clamped onto the heater with electrical probe tips making electrical contact. Above the detector is the electroplated Am-241 source with copper shutter.

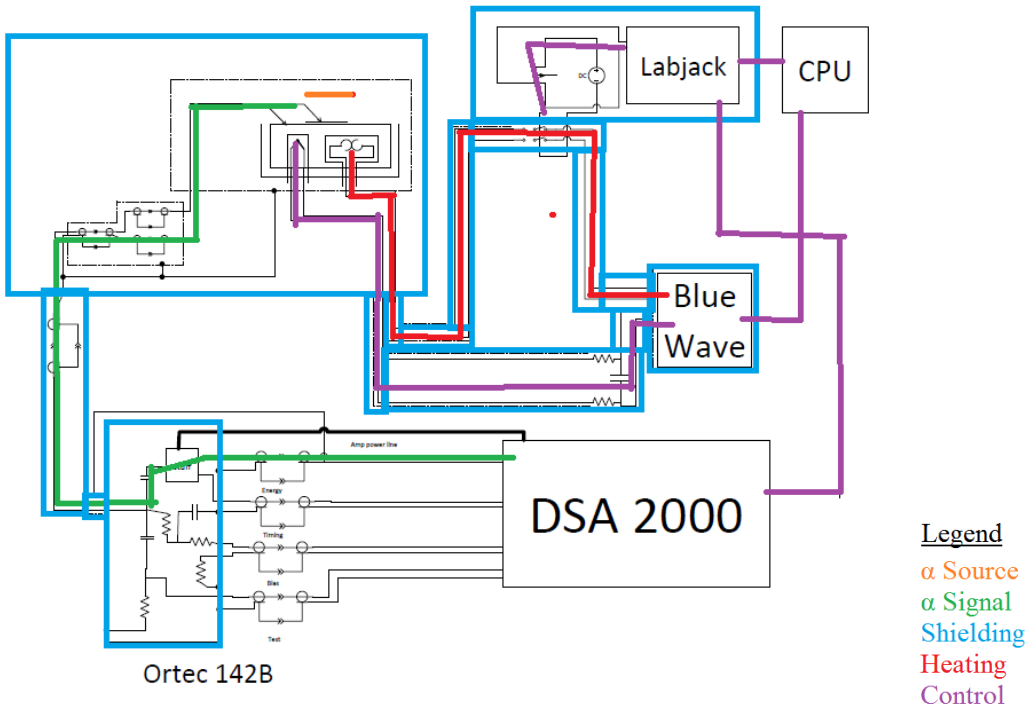

Figure 5: Illustration of the bell jar setup in the alpha spectroscopy configuration.

The Blue Wave semiconductor heater maintains temperature by measuring the temperature of the Inconel heater source through a thermocouple, and then electrically powering a heater installed in the Inconel heater surface. Since the charge-sensitive preamplifier has an effective gain of 80,000, the noise that the Blue Wave inserts through these two electrical feedthroughs may pass regulations on noise, but will be picked up in the spectroscopy setup. Thus, the Labjack controller shuts down the DSA 2000 taking counts by initiating an Inhibit signal. This leads to the fact that the temperature must oscillate in order to have time during which alpha particles can be counted. The heater controller is tuned so that the temperature oscillations are no more than +/- 5 °C.

When a device is tested, four different measurements occur. At a set bias voltage, an Am-241 spectrum is measured. Then, the shutter is moved so the Am-241 alpha particles cannot make it to the detector. Then, the Ortec pulser is turned on, and the pulser spectrum is measured. The applied bias voltage is turned off, and the preamplifier is switched off for the Keithley 2410 sourcemeter. Then, one I-V measurement is taken in the range of -1 V to +1 V, with a voltage step of 0.01 V. Finally, one I-V measurement is taken in the range between -300 and -200 V to 0 V, with a voltage step of 1 V.

During the spectra measurements, the detector was initially operated at 200 V at all temperatures. This value was determined by two methods; the first method estimated the voltage to fully deplete the epitaxial layer past the range of the Am-241 alpha particles in 4H-SiC using an average value for the dopant concentration in the epitaxial layer; the second method took a charge collection efficiency curve by increasing the voltage applied to the detector to the point where the charge collected no longer increased, and using the resulting voltage. Both methods yielded a little less than 200 V, but 200 V was chosen as a rounded number. Initial testing showed that this voltage was sufficient at room temperature, but was later found to be insufficient at elevated temperature due to increased thermal resistance in the equipment.

Two spectra taken from one of the detectors at 23 °C and 450 °C are shown in Figure 6. The effect of increasing temperature on the detector seems to be twofold: 1.) the centroid of the Gaussian peak position shifts; and, 2.) the FWHM of the Gaussian peak position increases with temperature.

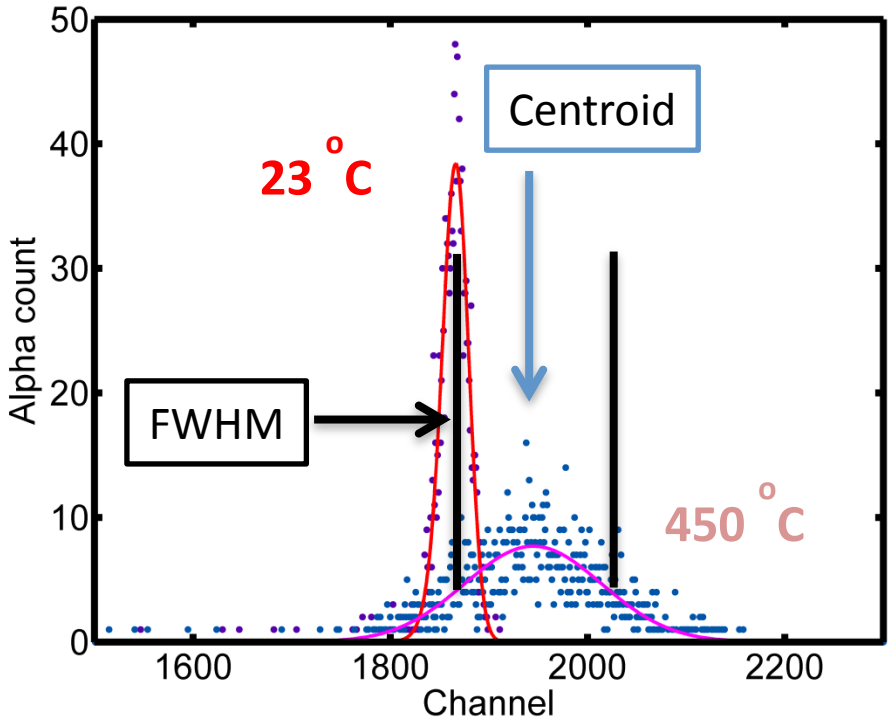

Figure 6: Two annotated spectra taken with one of the detectors tested at two different temperatures, 23 °C and 450 °C.

Figure 7 shows a plot of the location of the centroid of the Gaussian fit to the 5.388 MeV alpha line. Data are shown from different detectors, taken at varying voltages. At temperatures below 200 °C, the 5.388 MeV Gaussian peak centroid shows a relatively small shift upwards in channel number with temperature. Above 200 °C, a much ore significant upwards shift has been found for some of the experiments performed, while other experiments found a downward shift.

To explain these effects, we started from the fact that the bandgap of 4H-SiC (and any semiconductor) decreases with increasing temperature. A black line is drawn on Figure 7 corresponding to the upward trend one would expect given this decrease in bandgap. After analyzing the experiments performed, it was found that these experiments for which the centroid of the Gaussian peak lies along this line were performed with a bias voltage that was high enough to fully bias the detectors past the range of the Am-241 alpha particles in 4H-SiC. Those experiments for which the centroid of the Gaussian peak lies below this line were performed with a bias voltage that was not sufficient to fully bias the detectors past the range of the Am-241 alpha particles in 4H-SiC, as the following analysis showed.

Based on I-V measurements of the detector at high temperature, it was determined that at higher temperatures, the detector exhibited an increase of leakage current. At temperatures above 300 °C, the applied bias voltage of 200 V was increasingly being dropped across the 100 MΩ bias resistor in the Ortec 142B preamplifier due to Ohmic ($V = IR$) loss. Once this was identified as a possible mechanism for the Am-241 Gaussian peak shifting to lower channels, two methods were employed to compensate for this effect. For the first method, the temperature was held at 350 °C and 400 °C, and the voltage was increased until the centroid shift plateaued; this method is limited by the rating on the

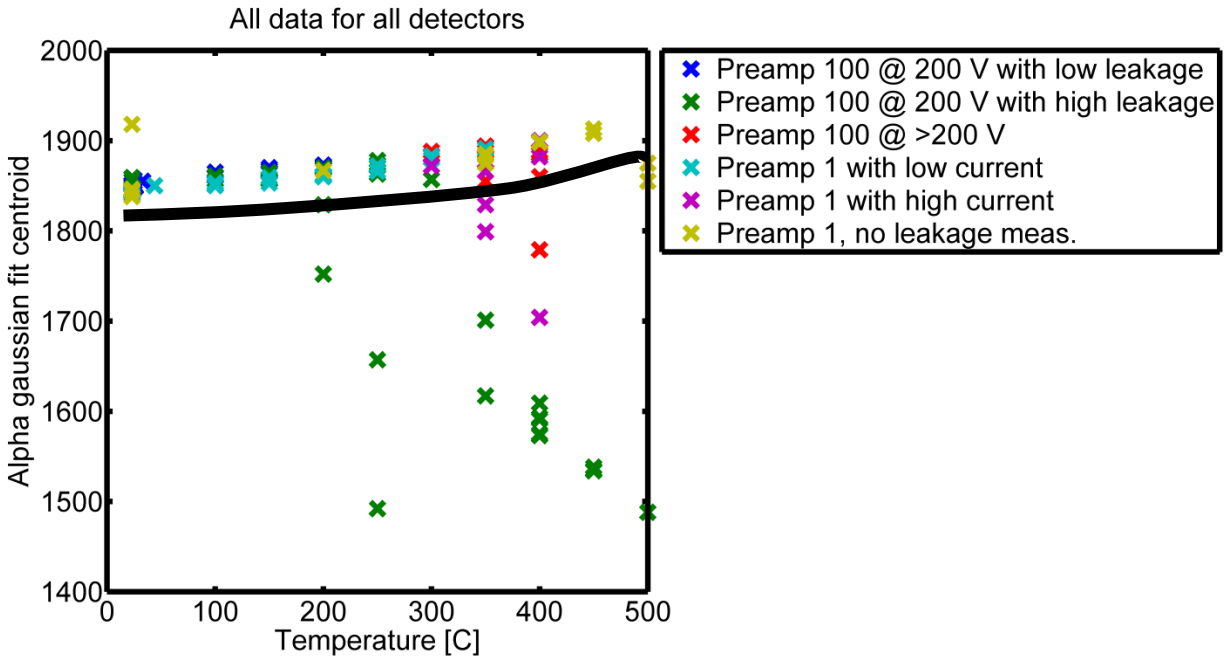

Figure 7: Plot of the Am-241 5.388 MeV alpha peak versus temperature. X's indicate measurement values. The black line indicates a trend with respect to temperature assuming that the peak follows the inverse of the bandgap versus temperature. X's that do not fall close to the black line indicate alpha spectra that were taken with an insufficient applied bias voltage.

maximum voltage the Ortec 142B preamplifier can supply. For the second method, a second Ortec 142B preamplifier was opened and modified so that the 100 MΩ bias resistor became an effective 1 MΩ bias resistor, and the effective Ohmic loss due to that bias resistor was reduced by 2 orders of magnitude. This preamp was labeled 'Preamp 1'. Figure 7 contains results from both preamplifiers.

Figure 8 shows the FWHM of the detector, in channels, versus the temperature of the detector. Note that detector #3 and #12 have significantly large FWHM below 250 °C when compared to the other detectors, indicating that these detectors had faults. Above 250 °C, where only the fault-free detectors operated successfully, the FWHM increases with increasing temperature. In-

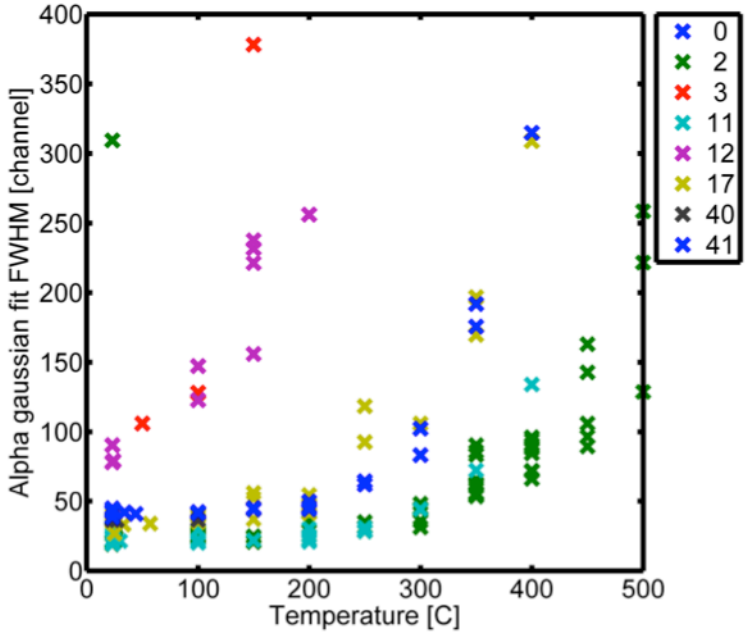

Figure 8: Plot of Am-241 FWHM versus temperature. X's indicate measurement values. The legend indicates detector numbers assigned in two ways: for numbers less than 30, assigned by Kadco Ceramics at time of dicing; for numbers greater than 30, assigned at time of metallization at Nanotech West.

crease of FWHM occurs for both an applied voltage of 200 V, and an applied maximum voltage.

Characterization Experiments:

Figure 9 shows a sample of I-V measurements that were performed in the bell jar experimental setup, using the Keithley 2410 sourcemeter. As the temperature of the detector increases, the current that is measured correspondingly increases. This occurs in both the forward-bias, and the reverse-bias regions.

Figure 10 shows an I-V plot for detector #2, which repeats the trend of higher measured current at higher detector temperature. For almost every data point in Figure 8 there are corresponding measurements taken from -1V to +1V and from 0 V to -200 or -300 V.

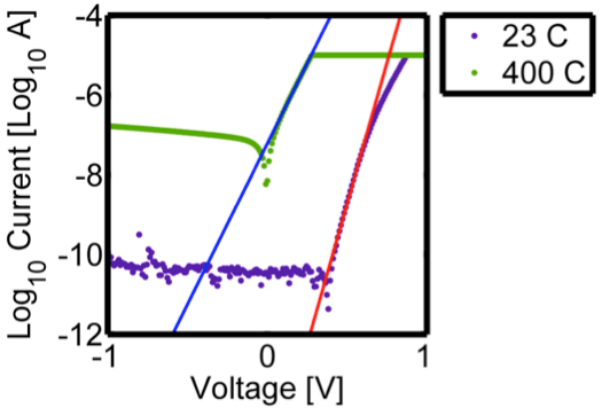

Figure 9: Plot of Log10(current) versus applied voltage for Detector #2 for 23 °C and 400 °C operation. Ideally, the forward-bias region should follow a straight line. The accuracy of the Keithley 2410 sourcemeter is limited to above Log10(current) = -10. The straight line at Log10(current) = -5 is due to a protection circuit in the Keithley 2410 sourcemeter, which prevents the current flowing through the detector under test, and protecting the test sample from being burnt out.

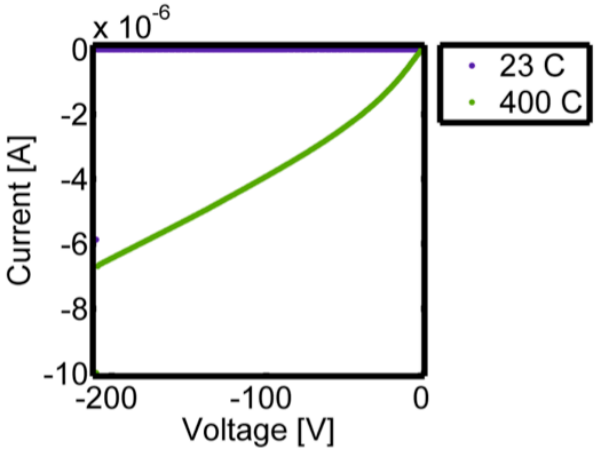

Figure 10: Reverse bias I-V plot for Detector #2 for 23 °C and 400 °C operation. As in Figure 7, the higher temperature measurement produces a high amount of current.

Figure 11 shows a plot of the saturation current of the tested detectors. As the temperature increases the saturation current increases for all of the successfully tested detectors. Figure 12 shows a plot of the absolute value of the leakage current at 200 V. In both cases, a lower amount of current corresponds to a detector with a smaller FWHM. This corresponds to well-known theory concerning Schottky diode-type detectors.

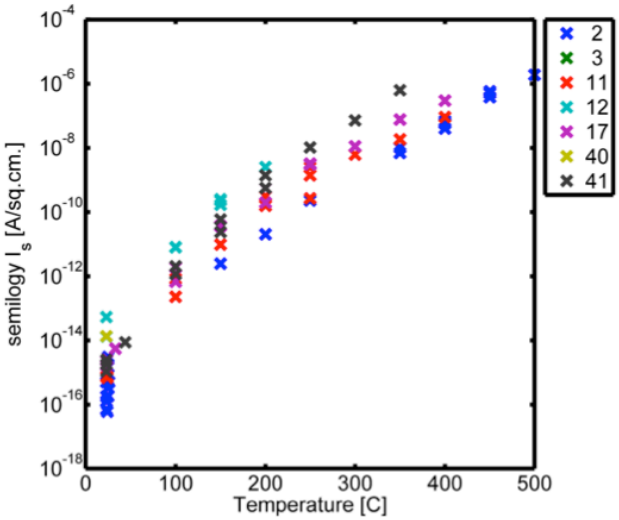

Figure 11: Semilog plot of I_s vs. temperature.

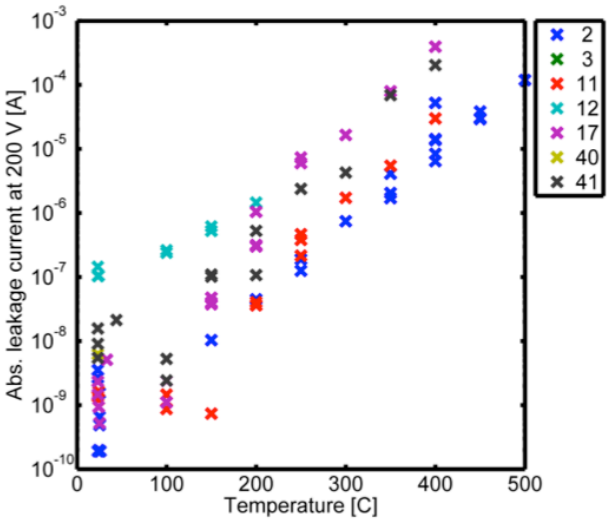

Figure 12: Leakage current at 200 V**.**

Ab-initio modeling:

Interaction with the radiation causes formation of various types of defects in 4H-SiC, such as point defects like silicon and carbon antisites, their vacancies and respective interstitials, dislocations, stacking faults, etc. Ab-initio modeling based on Density Functional Theory (DFT) has been employed to calculate the energetics of the various point defects. We employ PAW potentials within DFT to calculate the defect formation energies. We have developed a more thermodynamically correct approach to calculate

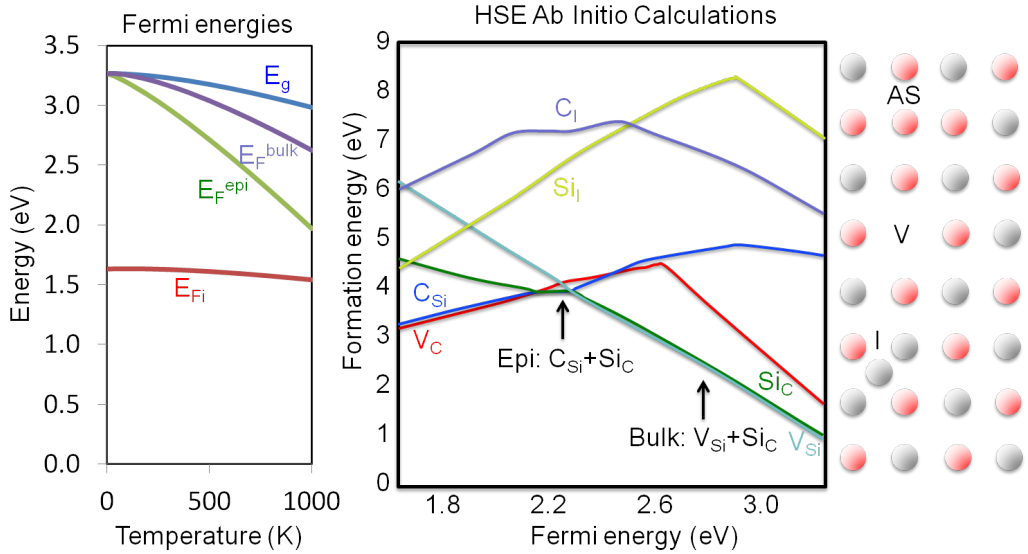

Figure 13: (a) Variation in the band gap and the Fermi level with increasing temperature. Bulk represents the highly n-type doped bulk region, while epi stands for the low doped n-type epilayer and 'I' for intrinsic. (b) Defect formation energies in the n-type region of 4H-SiC, calculated with high-accuracy "HSE" type density functional theory, for silicon and carbon vacancies (V_{Si} and V_C), respective interstitials (Si_i and C_i) and their antisites (Si_C and C_{Si}). (c) Schematic showing the various point defects considered in the formation energy calculation, using a novel method that allows accurate calculation of the chemical potentials needed [Rohan Mishra, Oscar D. Restrepo, Ashutosh Kumar, and Wolfgang Windl, J. Mater. Sci. 47, 7482-7497 (2012).].

the chemical potentials which are needed to calculate the formation energies. This method has also been successfully applied to other systems, such as InP [Rohan Mishra, Oscar D. Restrepo, Ashutosh Kumar, and Wolfgang Windl, J. Mater. Sci. 47, 7482-7497 (2012)]. Figure 13(a) shows the variation in the band gap and the Fermi energy in the various 4H-SiC layers as a function of doping. Figure 13(c) shows the schematic structure of the different point defects which are considered for formation energy calculations. 'V' represents vacancies, 'I' stands for interstitials and 'AS' for antisites. Figure 13(b) shows the calculated formation energies of various defects in SiC as a function of the Fermi level. It can be seen that in the highly n-type bulk region, silicon vacancies and silicon antisites maintain the stoichiometry, while for lower Fermi levels, both the antisites balance the stoichiometry, followed by compositional compensation of carbon antisites by carbon vacancies.

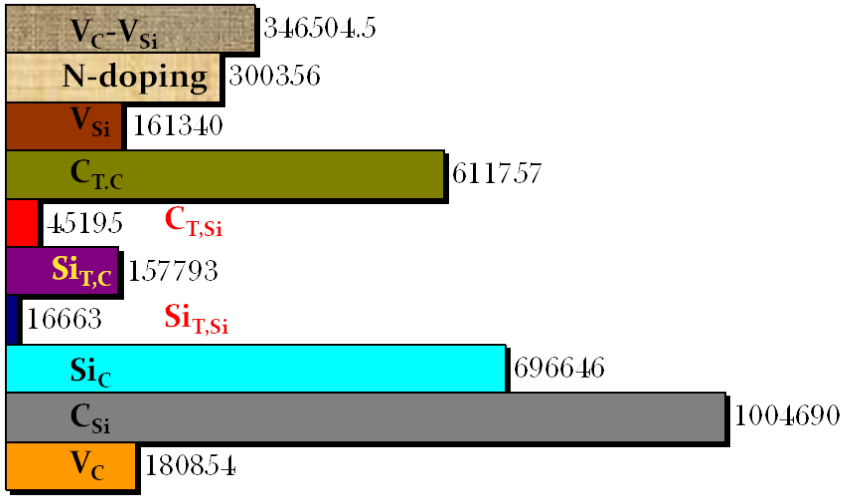

Figure 14: Effect of various defects on the carrier mobility in 4H-SiC

The defect formation energies are the major factor determining the stability of the different defects for a given Fermi level. As shown in Fig. 13, interstitials are observed to be less stable while antisites and vacancies are the most stable defects.

Since point defects act as scattering centers for conduction electrons, these defects affect the carrier mobility in the material to different degrees. Following Restrepo et al. [Appl. Phys. Lett. **94**, 212103 (2009)], we calculated the effect of various defects on the electron mobility employing a parameter free self-consistent mobility calculation within DFT. Figure 14 shows the calculated electronic mobility for a defect concentration of $1X10^{16}$ cm^{-3}. It can be seen that the unstable interstitials affect the carrier mobility most adversely, while antisites are the least harmful defects for the electrical conductivity in SiC. To understand the overall effect of radiation damage on the carrier mobility, the project plan included investigating the types of defects present with EELS modeling in comparison to experiment and their concentration with the help of damage

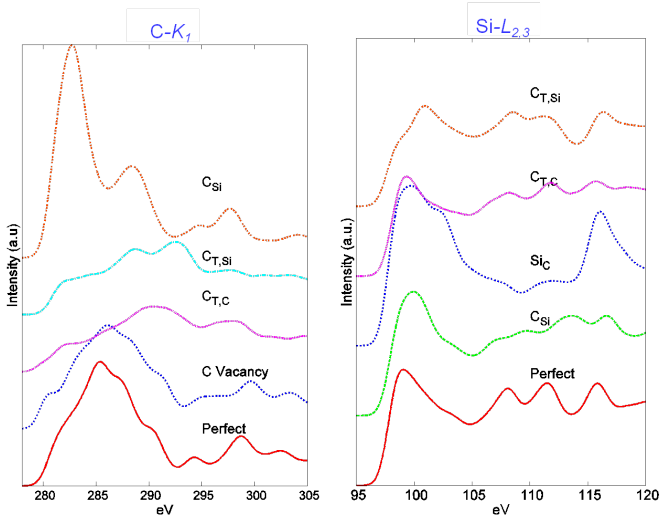

Figure 15: (a) C-K_1 edge and (b) Si-$L_{2,3}$ edge in SiC in presence of various defects calculated using Z+1 approximation within DFT.

evolution modeling. Figure 15 shows modeled EELS spectra for the C-K_1 and Si-$L_{2,3}$ edges for different types of defects in comparison to the respective edges in perfect SiC. Figure 15(a) shows that a carbon vacancy does not affect the C-K_1 edge structure of the nearest carbon atoms (which are 2nd neighbors), while a C-interstitial or antisite affects it significantly. An antisite causes a peak shift to lower energies with increased intensity, while an interstitial flattens the peak and shifts it to higher energies. Similar changes can be seen in Figure 15(b) for the Si-$L_{2,3}$ edge. The second and third peak is missing in the presence of a Si_C antisite defect while there is a shoulder near the main peak. The main peak position does not move but the shape of the spectrum changes. Comparison of these calculated spectra with experimental measurement will be helpful for determining the defect types present in the system.

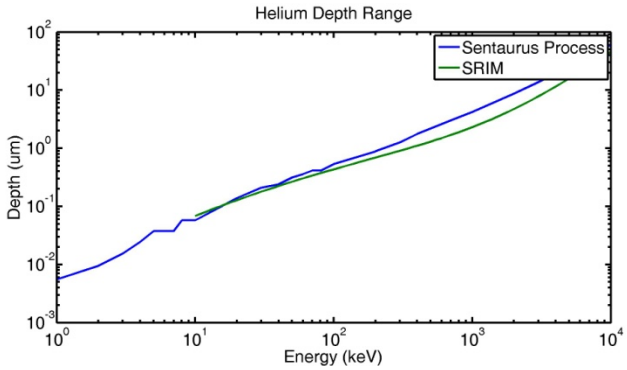

Figure 16: Comparison of SRIM and Sentaurus MC for damage depth distribution in 4H-SiC.

Damage evolution model:

Interaction with radiation creates damage in 4H-SiC in the form of point defects, stacking faults etc. As can be seen in Figure 13, some of the defects affect the functional properties of the material adversely, and the overall magnitude of this effect depends on the quantity of the defects present. In order to determine the overall change in the mobility, which also is an important input to our device modeling in case the effect is large, we employ damage evolution modeling using a continuum method to study the defect concentrations created by irradiation and their evolution with time as a function of ambient temperature. The choice of continuum modeling over kinetic Monte Carlo modeling allows focusing on longer-time evolution and steady-state concentrations, which are the important scales for operation of the detectors in an electrorefining environment, but may miss some detail and effects stemming from non-overlapping localized damage plumes.

Sentaurus Process MC along with SRIM was employed to create damage profiles in 4H-SiC. SRIM considers the material as amorphous, which avoids channeling effects, but is extremely well calibrated otherwise for a wide variety of materials including SiC, while Sentaurus Process MC treats materials as crystalline, but has been calibrated to a lesser degree for SiC (since it mostly focuses on Si devices). Therefore, we employed both codes to compare and optimize the damage profiles (Figure 16). To complement this damage creation simulation with continuum-level thermal-evolution modeling, a PROMIS license was obtained through a collaboration with Dr. Peter Pichler at the Fraunhofer Institute for Integrated Systems and Device Technolgy in Erlangen. A model for 4H-SiC has been written but is currently still in the process of optimization.

The governing equation for our PROMIS model for *N* defects of type *i* are

$$\sum_{j=1}^{N} \alpha_{ij} \cdot \frac{\partial W_j}{\partial t} + div\,\vec{J_i} + \gamma_i = 0; \quad i = 1 \ldots . N$$

where the first term determines the interaction/recombination between the defect *i* and other defects *j* and γ_i are the generation terms. The diffusion currents, $\boldsymbol{J}_i$ are given by

$$\vec{\boldsymbol{J}}_{\boldsymbol{i}} = \sum_{j=1}^{N} \left(a_{ij} \cdot \nabla W_j + b_{ij} \cdot W_j \cdot \nabla \varphi + c_{ij} \cdot W_j \right) + d_i$$

The boundary conditions applied use the interface to the Schottky metal as annihilation site to enforce equilibrium defect concentrations. The coefficients will be treated as functions of temperature, time and positions.

Device Modeling:

The drift-diffusion model of charge transport in semiconductors was applied in the Technology Computer Aided Design (TCAD) level device simulations. This model assumes that the charge carriers (electrons and holes) are near the edges of the band gap of the semiconductor, thus allowing approximations to be made for the coefficients of the charge transport equations. The equations governing the drift diffusion model are given as

$$\nabla \cdot \overrightarrow{J_n} = q(G_{Total} - R_{Total}) + q\frac{\partial n}{\partial t} \quad (1)$$

$$\nabla \cdot \overrightarrow{J_p} = -q(G_{Total} - R_{Total}) - q\frac{\partial p}{\partial t} \quad (2)$$

$$\overrightarrow{J_n} = qn\mu_n\vec{E} + qD_n\nabla n \quad (3)$$

$$\overrightarrow{J_p} = qp\mu_p\vec{E} - qD_p\nabla p \quad (4)$$

$$\nabla \cdot \varepsilon_s\vec{E} = (n + N_A - p - N_D) + \rho \quad (5)$$

where n and p are the concentrations of electrons and holes in units of number/cm^3, $\overrightarrow{J_n}$ and $\overrightarrow{J_p}$ are the electron and hole current fluxes, in units of A cm^{-2}, G_{Total} is the sum of all generation components in units of number cm^{-3}s^{-1}, R_{Total} is the sum of all recombination components in units of number cm^{-3}s^{-1}, μ_n and μ_p are the electron mobility and hole mobility, respectively, D_n and D_p are the electron diffusion coefficient and hole diffusion coefficient in units of cm^2 s^{-1}, respectively, $\vec{E}$ is the electric field, ε_s is the permittivity of the bulk material, N_A and N_D are the ionized acceptor and donor concentrations in units of number cm^{-3}, and ρ is the static charge concentration in units of number-cm^{-3}. In this model, the variables n, p, and $\vec{E}$ are allowed to vary in both space and time. The Einstein relationship is used to calculate D_n and D_p. The parameters μ_n, μ_p, G_{Total}, and R_{Total} not only vary in both space and time, but are parameterized in terms of n, p, and $\vec{E}$, yielding a nonlinear system of equations.

As shown in Figure 17, the device simulated was based on a 300 µm thick bulk SiC region doped to a donor concentration (N_D) equal to 10^{18} cm^{-3}, covered on the Si face with a 20 µm thick epitaxial layer

doped to N_D equal to 5x10^{14} cm^{-3}. The Schottky contact metal was modeled as an infinitely-thin (from the standpoint of alpha particle energy loss) nickel-based contact, with a metal workfunction of 1.8 eV. The alpha particle was assumed to strike the detector at the transverse (*x*)-midpoint of the Schottky contact, with an angle of incidence ϑ as measured from the surface normal (*n*) as shown in Figure 17. The coordinate *y* denotes a distance from the Schottky contact-epitaxial layer interface as measured along the normal. The location of the alpha particle along the alpha particle path as measured from the Schottky contact-epitaxial layer interface is denoted by the symbol l. The symbol u denotes a distance from the alpha particle path as measured along the normal to the alpha path. The symbol v also denotes a distance from the alpha particle path as measured along the normal to the alpha path, and together with u and *l* define distances along coordinates in a Cartesian coordinates system. The approximate reverse bias voltage to completely deplete the epitaxial layer is 200 V. The bias voltage was set to 400 V for all of the simulations, so for all calculations the detector was fully depleted. This was done to ensure that the detector was operated well into the fully reverse biased region of the *I-V* curve.

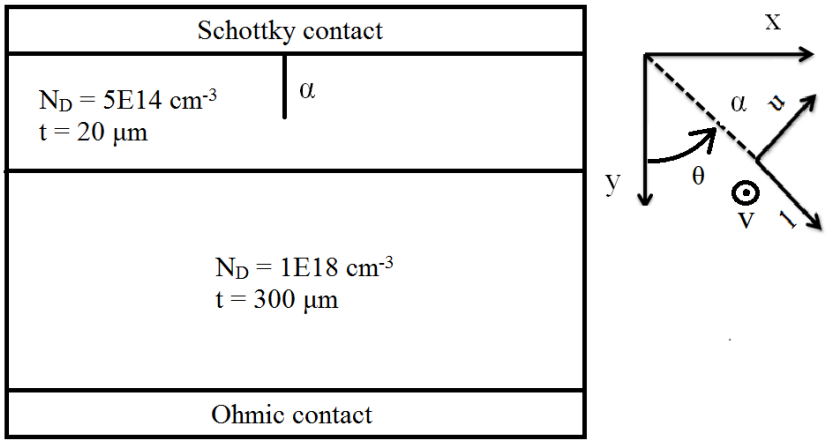

Figure 17: The geometry of the calculation along with parameters describing the detector**.**

A 3-dimensional form of the charge carrier (electron and hole) generation concentration profile $\left(G(l,u,v)\right)$, the number of electron-hole pairs generated per unit volume, that has been used by other investigators' in their simulations for perpendicularly incident charged particles has the form

$$G_{3D}(l,u,v) = \frac{LET_{SRIM}(l)}{\varepsilon}\frac{1}{\pi\sigma_r^2}exp\left[-\frac{u^2+v^2}{\sigma_r^2}\right] \tag{6}$$

where $LET_{SRIM}(l)$ is the energy deposited per unit path length as calculated using SRIM 2010, ε is the average energy to create an electron-hole pair, σ_r , l , u and v are as they were defined previously. In the simulations described herein a 2-dimensional analog of the 3-dimensional charge carrier (electron

and hole) generation concentration profile was used. The 2-dimensional concentration profile was assumed to have the form

$$G_{2D}(l,u) = \frac{LET_{SRIM}(l)}{\varepsilon}\frac{K}{\sigma_r}\frac{1}{\sqrt{\pi\sigma_r^2}}\exp\left[-\left(\frac{u}{\sigma_r}\right)^2\right] \quad (7)$$

As is the case for the charge carrier generation concentration profile $G_{3D}(l,u,v)$, the 2-dimensional concentration profile $G_{2D}(l,u)$ has dimensions of number of ionized charge carrier pairs per unit volume. *K* is a dimensionless adjustable parameter that was used to reduce the error that was induced by treating 3D ionization track structure evolutions using 2D simulations.

To check charge conservation, we integrated the generation terms over the dimensions perpendicular to the direction of the alpha particle; u and v in the case of a 3D simulation, or u in the case of a 2D simulation. Taking the integral for the 3D case,

$$\iint G_{3D}(l,u,v)dudv = \frac{1}{\varepsilon}LET_{SRIM}(l) \quad (8)$$

as it must. Similarly, taking the integral for the 2D case,

$$\int G_{2D}(l,u)du = \frac{1}{\varepsilon}\frac{K}{\sigma_r}LET_{SRIM}(l) \quad (9)$$

which differs from the integral of the 3D profile by a factor of K/σ_r. Thus, in order to have charge conservation, any concentrations or currents calculated using the 2D method were scaled by a factor of σ_r/K to be comparable to the results of a 3D simulation. These integrals also indicate that the 2D simulation had a virtual thickness of σ_r/K in the dimension v .

The charge carrier concentration distribution $G_{2D}(l,u)$ was implemented into the TCAD model of the detector. The structure mesh was defined by the Sentaurus mesh code with the minimum cell size specified as 2 nm in both height (*y*) and length (*x*) and with the maximum cell size specified as 5 nm in both height and length, with increasing mesh coarseness away from the track axis. This yielded a total simulation mesh with about 8x10^5 cells. Figure 18 shows the generated meshes for both a 0° alpha strike and a 45° alpha strike.

The main effects being investigated using this model are the charge carrier generation due to the alpha particle strike, and the recombination of charge carriers after being generated, and before being collected at the metal contacts. The charge carrier generation due to the alpha particle strike contributes to the G_{Total} term, while the recombination of charge carriers after being generated, and before being collected at the metal contacts, contributes to the R_{Total} term.

Auger recombination is a three-particle recombination process, wherein an electron-hole pair recombines, with the excess energy given to a third charge carrier which is then free to thermalize. The third charge carrier can either be an electron, or a hole, and is described using

$$R_{\text{Auger}} = \left(C_{n,\text{Auger}} n + C_{p,\text{Auger}} p\right)\left(np - n_i^2\right) \tag{10}$$

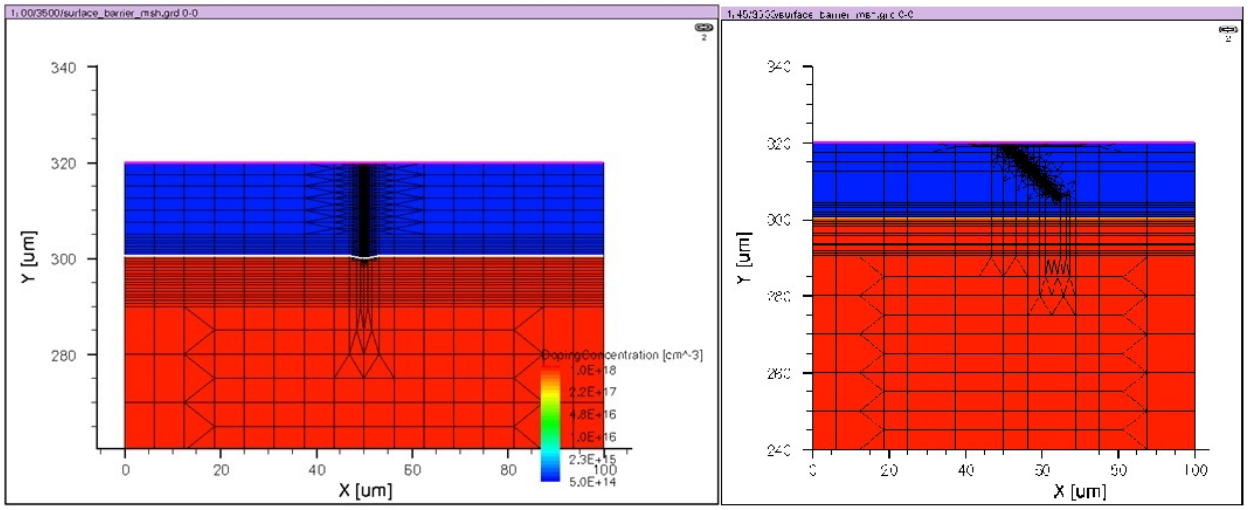

Figure 18: Calculational mesh for a 0° alpha strike, shown left, and a 45° alpha strike, shown right. Blue indicates the epitaxial layer and red indicates the substrate.

where n_i is the intrinsic carrier concentration, and $C_{n,\text{Auger}}$ and $C_{p,\text{Auger}}$ are the electron-based and hole-based Auger recombination coefficients. To simplify the calculations, it was assumed that $C_n = C_p$, and thus the ambipolar Auger recombination coefficient C_a is defined as $C_a = C_n = C_p$. Quantifying the individual recombination coefficients is beyond the scope of this project. Thus, the expression for R_{Auger} can be rewritten as

$$R_{\text{Auger}} = C_a(n + p)\left(np - n_i^2\right) \tag{11}$$

The change in detector output with respect to radiation damage has not yet been implemented into the TCAD model. Radiation damage effects can be implemented in the TCAD model by changing the electron and hole mobilities, μ_n and μ_p, including damage-assisted recombination into the total recombination R_{Total}, and including charge trapping via crystal defects.

Figure 19 shows the pulses obtained from the TCAD simulation of the detector for K = 1. Five different simulations are shown for the angle of incidence θ = 0°, in which the energy of the alpha particle was varied from 3500 keV to 5500 keV, and the detector temperature was held at room temperature. As the energy of the alpha particle increases, the peak current of the output pulses increase. Figure 20 shows the results of a 5500 keV alpha strike, with θ values of 00°, 30°, 45°, and 60°. As the particle strike becomes more grazing, the shape of the trace of current collected versus time changes. As the angle of incidence becomes more grazing, the peak current decreases, and the rise time increases; that is, the length of time from the onset of current to the peak current increases.

Figure 21 shows the charge collection results of a 5500 keV alpha strike simulation, with an angle of incidence θ = 0°, and the detector operation temperature T varying from 27 °C to 627 °C, in increments

of 100 °C. As the detector operation temperature increases, the amount of charge collected decreases. The data sets are both fit to an exponential function that decreases with increasing temperature. Figure 22 shows the amount of charge lost to auger recombination versus detector operation temperature. As the detector temperature increases, the amount of charge lost to auger recombination increases. This is because, as temperature increases, both the electron and hole mobilities decrease, which slows the moving charge carriers as they leave the detector. This allows more charge to be lost due to auger recombination, before the charge carriers can exit the detector.

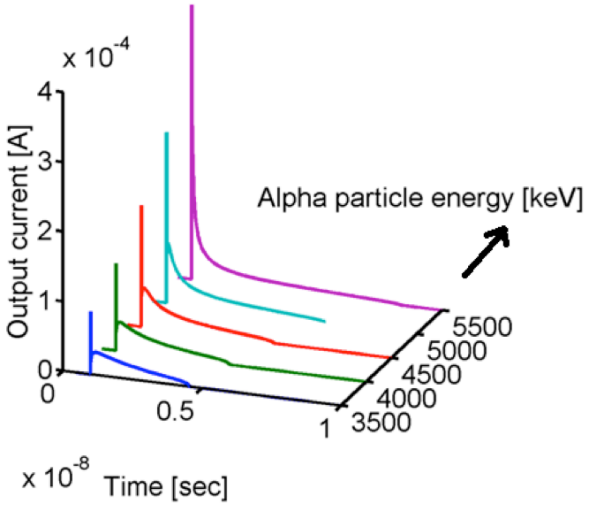

Figure 19: Output pulses for simulations where the energy of the incident alpha particle ranged from 3500 keV to 5500 keV for K = 1.

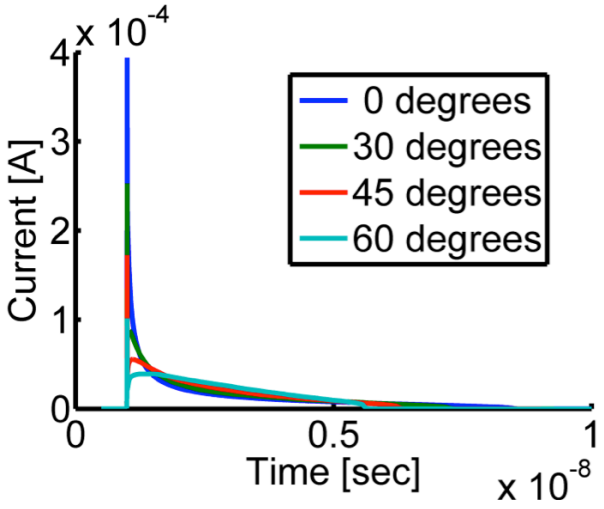

Figure 20: Output pulses from simulations where the angle of incidence of a 5500 keV alpha particle was varied from 0 to 60° for K = 0.43.

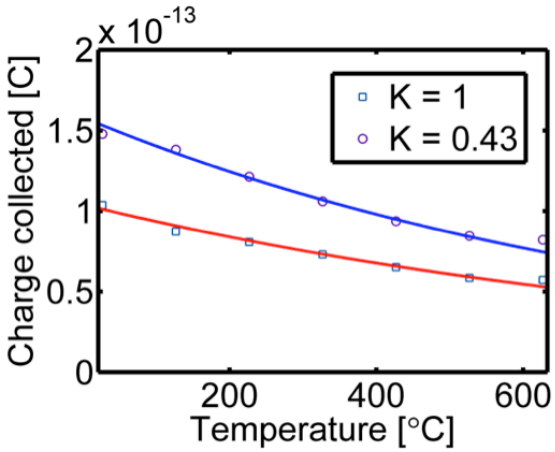

Figure 21: Total charge collected for an incident alpha particle strike with energy 5500 keV, with

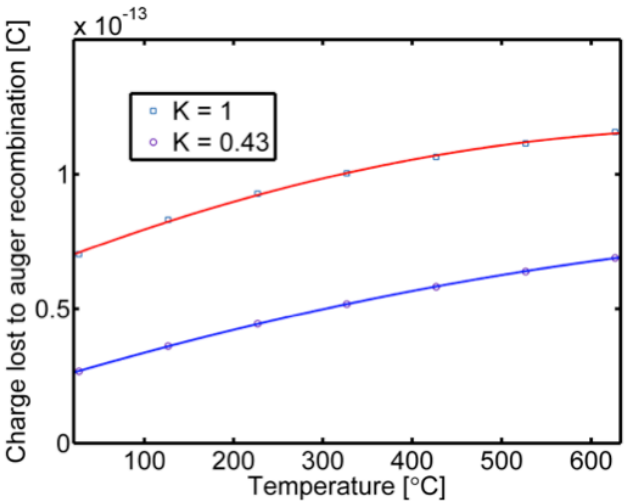

Figure 22: Total charge lost to auger recombination for an incident alpha particle strike with energy 5500

an angle of incidence θ = 0°, and varying temperature of operation from 27 °C to 627 °C.

keV, with an angle of incidence θ = 0°, and varying temperature of operation from 27 °C to 627 °C.

In comparing Figure 21, which shows the modeling results, to Figure 7, which describes the experimental results, it is obvious that the observed trends with respect to temperature do not agree. At the time these calculations were performed, the experimental results were not yet collected, and so a model that was well-calibrated to the physical results was not available and its development is subject to future work.

Underachieved milestones:

EELS measurements: Electron Energy Loss Spectroscopy measurements of pre and post-irradiated 4H-SiC devices was proposed to identify defects in the material in comparison with the calculated spectra. However, the EELS experimental measurements could not be performed. The FEI-TITAN Microscope at OSU was out of service for a long time, whereupon we tried to perform the EELS measurements in collaboration with Oak Ridge National Laboratory. Samples were irradiated on December 2010, and sent to PRNL via mail but unfortunately, during irradiation the SiC wafer piece had shattered, and the samples were too small and unsuitable for TEM. Samples were again irradiated in March 2011 and sent to ORNL via mail but unfortunately were lost in mail. Another set of samples were irradiated in June 2011 and sent to ORNL. Unfortunately this time again, the samples did not reach their destination. Due to budgetary limitations, further irradiations for EELS measurements were dropped, so validation with calculated EELS measurements remain an underachieved milestone of the project.

KMC modeling: KMC modeling had been proposed to study short-time scale events occurring in localized, non-overlapping damage plumes, more or less independent of each other, such as defect recombination occurring just afterdamage creation, typically within the first few picoseconds. However, since the overall dimension of the device in our project was large and defect evolution during long time operation was the central goal, the team focused on a continuum based model which is more appropriate to model over long time scale. Therefore, the idea of KMC modeling was dropped, and defect evolution was modeled on the continuum level in collaboration with Dr. Peter Pichler from the Fraunhofer Institute for Integrated Systems and Device Technology, Erlangen, Germany who is a renowned expert in process modeling in semiconductors. Interaction with radiation creates damage in 4H-SiC in terms of point defects, stacking faults etc.

Irradiation experiments: Reactor tests of the devices have not yet been performed. To test the detectors with an extended alpha particle source, a thick irradiator material will be placed directly in contact with the Schottky contact of the detectors. This irradiator material will contain a material that contains an isotope which has a large (n,α) cross section. By irradiating this setup with thermal neutrons, a situation similar to the modeling of the pyroprocessing will be experimentally achieved. The biggest difference between the modeling results and the experimental results will be the alpha particle stopping power $dR(E')/dE'|_E$, and the initial particle energies E_i. Also, depending on the radioactive

isotope used in the reaction, a secondary particle is emitted along with the alpha particle. In using the $Li^6(n,\alpha)$ reaction, a triton is emitted. In using the $B^{10}(n,\alpha)$ reaction, a Li atom is emitted. In order to test the $Li^6(n,\alpha)$ reaction, 5 TLD-600's were purchased from Thermo Scientific. In order to test the $B^{10}(n,\alpha)$ reaction, BN wafers were purchased from Goodfellow. These will be ground down to size to fit into the detector holders discussed in the next paragraph.

By the end of the funding period, a prototype detector holder had been constructed. This holder has three purposes: 1) to hold the detectors and irradiation material in close contact; 2) to maintain electrical contact with the detector's Schottky and Ohmic metal contacts, allowing reverse biasing and signal collection while under irradiation; 3) to allow the detector to be held at high temperature during testing; and 4) to electrically shield the detector from external Electro-Magnetic Interference (EMI), and EMI originating from the heater, which was a significant issue during bell jar testing of the detectors. The first and second iterations of this holder have been machined, identified as Holder #1 and Holder #2, and potential issues identified in terms of electrical operation, mechanical construction, and radioactivity issues have been discussed with OSURR Ohio State University Research Reactor (OSURR) staff. Figure 23 shows a Solidworks model of the third iteration, identified as Holder #3. In order to minimize the amount of radioactivity produced by the detector holder during irradiation, the size of the detector holder was minimized while still maintaining the function of the holder, and the materials of the holder were chosen to minimize the wait time of decay of radioactive products until an experimentalist can safely handle the detector once outside of the test facility. For the detector holder body, aluminum was chosen due to its low neutron activation cross section, low cost, and relative ease at machining. Because aluminum readily oxidizes at elevated temperature, titanium was chosen as a second material for elevated temperature tests. Titanium was chosen for its high temperature operation, machinability, and resistance to oxidation at elevated temperature.

A SMA connector was used in place of more commonly-used BNC connectors. BNC connectors see wide use in applications where low cost is favored over high signal fidelity, due to the SMA connectors' higher cost and correspondingly higher cutoff frequency. As such, SMA connectors have become a workhorse of the RF community. BNC connectors are typically plated with Nickel, which raise issues with production of radioactive isotopes. SMA connectors typically come in two materials – brass body with beryllium-copper center pin, and steel body with steel center pin [18]. Radioactivity in a brass-body connector would decay faster than a steel-body connector, so it was chosen for the first test. The center pin is typically insulated from the outer conductor using PTFE, which drives the cutoff frequency slightly lower than a connector insulated with air. Because SMA connectors are smaller, they are able to be made with air as insulator. This correspondingly drives up the cutoff frequency, and also the cost. For an initial low-temperature test, the SMA connector with brass body and PTFE insulation will be used with an aluminum body. When high temperature irradiation is required, the SMA connector will be used. Note that the choice of connectors is not typically possible with BNC connectors, because the center pin would be not be supported well, and would likely be crushed by a small amount of offset when the connection is tightened by hand.

As shown in Figure 23, the 4H-SiC Schottky diode detector will be clamped into the base of the detector holder, and placed into a neutron field provided by the OSURR. Initial tests will be performed at different neutron fluxes, taking the resulting spectra, and correlating the observed radioactive particle source rates with the assumed neutron reactions at the different neutron fluxes. After initial

testing of this detector setup, the detector holder will be modified to allow clamping with an electrical heater. Initial testing of the detector setup with an electrical heater will be performed to observe the change in alpha spectra with respect to change in temperature, which is due to a change in the source material with respect to a change in temperature. At this point, the detectors will be irradiated to high fluence at high temperature to show the influence of damage on detector performance.

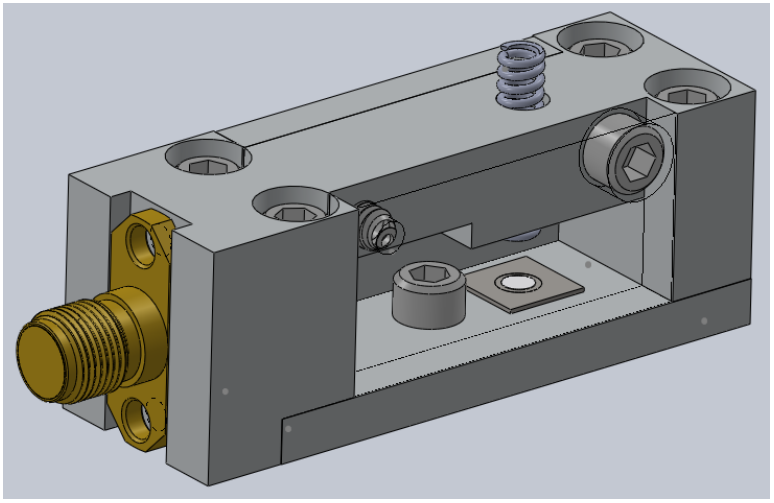

Figure 23: In-reactor detector holder. Shown is the SMA connector (brass) lacking a detailed model of the center pin, aluminum housing with side panel, bottom panel, and aluminum machine screws (silver), 4H-SiC detector (gray), B_4C irradiator disk (white), and compression spring (blue-gray). Not shown are the metal contact probe, which makes electrical connection to the Schottky contact, and alumina sheet, which insulates the aluminum metal contract probe from the compression spring and housing.

Conclusions:

In this project, we have designed a 4H-SiC Schottky diode detector device in order to monitor actinide concentrations in extreme environments, such as present in pyroprocessing of spent fuel. For the first time, we have demonstrated high temperature operation of such a device, in successfully detecting alpha particles. We have used AM-241 as an alpha source for our laboratory experiments. Along with the experiments, we have developed a multi scale model to study the phenomena controlling the device behavior and to be able to predict the device performance. Our multi scale model consists of ab initio modeling to understand defect energetics and their effect on electronic structure and carrier mobility in the material. Further, we have developed the basis for a damage evolution model incorporating the outputs from ab initio model in order to predict respective defect concentrations in the device material, which we hope to complete soon in following projects. Such a model is currently not available in the literature. Further, a fully equipped TCAD-based device model has been developed to study the phenomena controlling the device behavior. Using this model, we have proved our concept that the detector is capable of performing alpha detection in a salt bath with the mixtures of actinides present in a pyroprocessing environment.

Publications and Presentations

Authors:	Ashutosh Kumar, Oscar D. Restrepo, Wolfgang Windl
Title:	Ab-initio modeling of electronic structure and defects in 4H-SiC
Event:	2010 Ohio Innovation Summit, April 20-21, Columbus ,OH
Form:	Poster
Publication:	n/a

Authors:	Ashutosh Kumar, Oscar D. Restrepo, Wolfgang Windl
Title:	First principles calculations of electronic structure and mobility in 4H-SiC
Event:	2010 IMR Materials Week, Sept. 13 – 15, Columbus ,OH
Form:	Poster
Publication:	n/a

Authors:	Ashutosh Kumar, Oscar D. Restrepo, Wolfgang Windl
Title:	Atomistic modeling of the influence of irradiation on the electronic properties of 4H-SiC
Event:	2011 Hayes Graduate Forum, Mar. 4, Columbus ,OH
Form:	Poster
Publication:	n/a

Authors:	Ashutosh Kumar, Oscar D. Restrepo, Wolfgang Windl, Timothy Garcia, Alexandra Zelaski, Thomas E. Blue
Title:	Ab-initio studies of isolated defects, defect clusters and their effect on electronic mobility in 4H-SiC
Event:	2011 MRS Spring Meeting, April 24-29, San Francisco, CA
Form:	Oral
Publication:	n/a

Authors:	Ashutosh Kumar, Oscar D. Restrepo, Wolfgang Windl, Timothy Garcia, Alexandra Zelaski, Thomas E. Blue
Title:	Ab-initio calculations of defect energetic and electronic structure in 4H-SiC
Event:	2011 American Nuclear Society Annual Meeting, June 26-29, Hollywood, FL
Form:	Oral
Publication:	Transactions of American Nuclear Society, vol 104 pp 57-58 (2011)

Authors:	Ashutosh Kumar, Alexandra Zelaski, Timothy Garcia, Thomas E. Blue, Wolfgang Windl,
Title:	4H-SiC schottky diode radiation detectors for alpha-particle spectrometry in extreme environments
Event:	2011 IMR Materials Week, Sept. 12-14, Columbus, OH
Form:	Poster
Publication:	n/a

Authors:	Ashutosh Kumar, Oscar D. Restrepo, Wolfgang Windl, Timothy Garcia, Alexandra Zelaski, Thomas E. Blue
Title:	Ab-initio assisted study of irradiation effects on electronic properties of 4H-SiC
Event:	2011 MS&T conference, Oct. 17-20, Columbus, OH
Form:	Oral
Publication:	n/a

Authors:	Ashutosh Kumar, Oscar D. Restrepo, Wolfgang Windl,
Title:	Ab-initio study of effect of defects on the electronic mobility in 4H-SiC
Event:	IWCE-2012, May 21-25, Madison, WI
Form:	Poster
Publication:	Abstract in the Proceedings of IWCE-2012, pp 169-170

Authors:	Timothy Garcia, Thomas Blue, Wolfgang Windl
Title:	Continuum modeling of performance and radiation hardness in semiconductor-based radiation detectors
Event:	2010 OSU Materials Week, Sept. 13 – 15, Columbus ,OH
Form:	Poster
Publication:	n/a

Authors:	Timothy Garcia, Thomas Blue, Wolfgang Windl
Title:	Continuum modeling of performance and radiation hardness in semiconductor-based radiation detectors
Event:	MAE Graduate Student Research Day 2010, Oct. 15, 2010, Columbus, OH
Form:	Poster
Publication:	n/a

Authors:	Timothy Garcia, Thomas Blue
Title:	Continuum modeling of performance and radiation hardness in semiconductor-based radiation detectors
Event:	2010 Ohio Innovation Summit, Apr. 20-21, Columbus, OH
Form:	Poster
Publication:	n/a

Authors:	Alexandra Zelaski
Title:	
Event:	2010 Ohio Innovation Summit, Apr. 20-21, Columbus, OH
Form:	Poster
Publication:	n/a

Authors:	Timothy Garcia, Thomas Blue, Wolfgang Windl, Ashutosh Kumar, Alexandra Zelaski
Title:	SiC Schottky Diode Detectors for Measurement of Actinide Concentrations from Alpha Activities in Molten Salt Electrolyte
Event:	Then-Senator George Voinovich (R-OH) personal visit, Sept. 26, 2010, Columbus, OH
Form:	Poster
Publication:	n/a

Authors:	Timothy R. Garcia, Thomas E. Blue, Wolfgang WIndl
Title:	Computational alpha-particle Spectroscopy using TCAD for Pyroprocessing Monitoring
Event:	American Nuclear Society Annual Meeting 2011, Jun. 26-30, 2011, Hollywood, FL
Form:	Presentation
Publication:	Transactions of the American Nuclear Society

Authors:	Alexandra Zelaski, Timothy R. Garcia, Ashutosh Kumar, Thomas E. Blue, Wolfgang Windl
Title:	Development of 4H-SiC Schottky Diode Detector for Nuclear Fuel Reprocessing Applications
Event:	American Nuclear Society Annual Meeting 2011, Jun. 26-30, 2011, Hollywood, FL
Form:	Presentation
Publication:	Transactions of the American Nuclear Society

Authors:	Timothy Garcia, Alexandra Zelaski, Ashutosh Kumar, Thomas Blue, Wolfgang Windl
Title:	Continuum modeling of performance and radiation hardness in semiconductor-based radiation detectors
Event:	OSU 2011 Materials Week, Sept. 12-14, 2011, Columbus, OH
Form:	Poster
Publication:	n/a

Authors:	Timothy Garcia, Alexandra Zelaski, Ashutosh Kumar, Thomas Blue, Wolfgang Windl
Title:	Continuum modeling of performance and radiation hardness in semiconductor-based radiation detectors
Event:	MAE Graduate Student Research Day 2011, Oct. 7, 2011, Columbus, OH
Form:	Poster
Publication:	n/a

Authors:	Timothy R. Garia, Ashutosh Kumar, Alexandra Zelaski, Ben Reinke, Thomas E. Blue, Wolfgang Windl
Title:	TCAD modeling of SiC alpha-particle radiation detectors
Event:	IWCE-2012, May 21-25, 2012, Madison, WI
Form:	Poster
Publication:	n/a

Authors:	Timothy Garcia, Ashutosh Kumar, Ben Reinke, Thomas Blue, Wolfgang Windl
Title:	Modeling and experimentation of radiation hardness in semiconductor radiation detectors
Event:	NASA Future Forum, February 20-12, 2012, Columbus, OH
Form:	Poster
Publication:	n/a

Authors:	Timothy Garcia, Ashutosh Kumar, Ben Reinke, Thomas Blue, Wolfgang Windl
Title:	Modeling and experimentation of radiation hardness in semiconductor radiation detectors
Event:	ANS Winter meeting, November 11-15, 2012, San Diego, CA
Form:	Poster
Publication:	n/a

Authors:	Tim Garcia, Ben Reinke
Title:	SiC-Based Alpha Detectors for Electrochemical Applications
Event:	MPACT working group meeting, March 13-15, 2012, Savannah River National Laboratory
Form:	Presentation
Publication:	n/a

Authors:	Tim Garcia, Ashutosh Kumar, Ben Reinke, Thomas E. Blue, and Wolfgang Windl
Title:	SiC-Based Alpha Detectors for Electrochemical Applications
Event:	MPACT working group meeting, August 28-30,2012, Idaho National Laboratory
Form:	Presentation
Publication:	n/a

Authors:	Tim Garcia, Thomas Blue, Wolfgang Windl Ashutosh Kumar, Ben Reinke, Alexandra Zelaski
Title:	High temperature SiC alpha-particle detectors for pyroprocessing
Event:	ANS Annual Meeting, June 24-28, 2012, Chicago, IL
Form:	Presentation
Publication:	n/a

Authors:	Tim Garcia, Thomas Blue, Wolfgang Windl Ashutosh Kumar, Ben Reinke
Title:	Electrical characterization of high temperature SiC alpha-particle detectors for pyroprocessing
Event:	ANS Winter Meeting, November 11-15, 2012, San Diego, CA
Form:	Presentation
Publication:	n/a

Authors:	Wolfgang Windl
Title:	SiC–Based Alpha Detectors for Electrochemical Applications
Event:	FCR&D Annual Meeting, October 30 – November 1, Argonne National Laboratory
Form:	Presentation
Publication:	n/a

Authors:	Benjamin Reinke, Timothy Garcia, Ashutosh Kumar, Dr. Thomas Blue, Dr. Wolfgang Windl
Title:	Modeling and Experimentation of Radiation Damage at Cryogenic Temperatures in 4H-SiC and Fiber Optics Cable
Event:	NASA Future Forum, February 20-21, 2012, The Ohio State University, Columbus, OH
Form:	Poster
Publication:	n/a

Authors:	Benjamin Reinke, Timothy Garcia, Ashutosh Kumar, Dr. Thomas Blue, Dr. Wolfgang Windl
Title:	Modeling and Experimentation of Radiation Damage at Cryogenic Temperatures in 4H-SiC and Fiber Optics Cable
Event:	DOE Energy Frontier Research Center Summer School 2012, June 11-15, Knoxville, TN
Form:	Poster
Publication:	n/a

Authors:	Benjamin Reinke, Timothy Garcia, Ashutosh Kumar, Dr. Thomas Blue, Dr. Wolfgang Windl
Title:	Modeling and Experimentation of Radiation Damage at Cryogenic Temperatures in 4H-SiC and Fiber Optics Cable
Event:	The Ohio State University John Glenn School for Public Policy Nuclear Symposium, August 14, 2012, The Ohio State University, Columbus, OH
Form:	Poster
Publication:	n/a

Authors:	Benjamin Reinke, Timothy Garcia, Ashutosh Kumar, Dr. Thomas Blue, Dr. Wolfgang Windl
Title:	Modeling and Experimentation of Radiation Damage at Cryogenic Temperatures in 4H-SiC and Fiber Optics Cable
Event:	NASA Tech Days, November 28-30, 2012, Cleveland, OH
Form:	Poster
Publication:	n/a

Authors:	Benjamin Reinke, Timothy Garcia, Ashutosh Kumar, Dr. Thomas Blue, Dr. Wolfgang Windl
Title:	Modeling and Experimentation of Radiation Damage at Cryogenic Temperatures in 4H-SiC and Fiber Optics Cable
Event:	ANS Winter Meeting, November 11-15, 2012, San Diego, CA
Form:	Poster
Publication:	n/a